J IRAN CHEM SOC
DOI 10.1007/s13738-016-0991-y

ORIGINAL PAPER

Bisphosphoramidate derivatives: synthesis, crystal structure, anti-cholinesterase activity, insecticide potency and QSAR analysis

Khodayar Gholivand[1] · Ali Asghar Ebrahimi Valmoozi[1] · Mina Salahi[1] · Fatemeh Taghipour[1] · Elham Torabi[1] · Saied Ghadimi[2] · Mahboobeh Sharifi[3] · Mohammad Ghadamyari[3]

Received: 10 July 2016 / Accepted: 3 October 2016

Abstract A series of temephos (Tem) derivatives with the general structure of P(O)NH–X–NHP(O) (**1–22**) were synthesized and characterized by ^{31}P, ^{13}C, ^{1}H NMR and FT-IR spectral techniques. The electron density (ρ) value at the bond critical point (bcp) of P(1′)–O(1′)···(1)H–N(1) (0.040 e Å^{-3}) P(1)–O(1)···(1′)H–N(1′) (0.031 e Å^{-3}) as well as the stabilization energy of electronic delocalization of results of NBO analysis showed the hydrogen bonding energy in P(1′)–O(1′)···(1)H–N(1) model ($E^2 = -72.15$ kJ mol^{-1}) and P(1)–O(1)···(1′)H–N(1′) ($E^2 = -45.67$ kJ mol^{-1}) of the crystal cluster **7**. The activities of Tem derivatives were evaluated using the modified Ellman's method on cholinesterase (ChE) enzymes. The insecticide activity of Tem analogous appraised for the elm leaf beetle in which the **18** had more effective than the other compounds in inhibition α-esterase of insect. Principal component analysis–quantitative structure activity relationship (PCA–QSAR) models indicated that it was deduced that the frontier molecular orbital energy parameters in PC_1 are predominated from those related to electronic in PC_2 and structural parameters in PC_3 equation. Multiple linear regressions–QSAR models clarified that the molecular descriptors like an integrated net charge of nitrogen atom (Q_N), polarizability (PL_{N-H}) and lowest unoccupied molecular orbital (E_{LUMO}) proved important in defining the activity of the candidates.

Keywords Bisphosphoramidate · Temephos · Hydrogen bond · Cholinesterase inhibitor · QSAR

Introduction

Bisphosphoramidates (BPAs) are best known for their highly toxic effect as agricultural chemicals. BPAs with the general structure of P(O)NH–X–NHP(O) skeleton are important class of compounds that exhibit the insecticide properties to inhibit the cholinesterase acetylcholinesterase (AChE) enzymes [1, 2]. Little attention has been given to the interaction mechanism of the ChE enzymes and BPAs [3, 4]. The famously derivative in the BPAs category is attributed to temephos (Tem) pesticide because it is a useful insecticide to control the larvae of mosquitoes, midges and moths [5, 6]. However, Tem has side effects on human as anti-AChE and carcinogenic potential [7]. Therefore, designing and producing the selective compounds of Tem category having high insecticide potential with less anti-AChE and carcinogenic effects are required. To extend and to evaluate this problem, QSAR method has been introduced in order to overcome the inhibition mechanism [8]. The elm leaf beetle *Xanthogaleruca luteola Müll* is the most serious pest of the elm tree. Larvae feed on the parenchyma of leaves, without consuming the veins, and cause severe damage to trees. If the damage is severe and occurs several years in a row, the trees develop deformed canopies and suffer vigor loss, physiological disorders and reduced photosynthesis, which predispose them to the action of other pests, plant disease and stress factors. They become particularly susceptible to scolytid

✉ Khodayar Gholivand
gholi_kh@modares.ac.ir

[1] Department of Chemistry, Tarbiat Modares University, P.O. Box: 14115-175, Tehran, Iran

[2] Department of Chemistry, Imam Hossein University, Tehran, Iran

[3] Department of Plant Protection, Faculty of Agricultural Science, University of Guilan, Rasht, Iran

Published online: 20 October 2016

beetles carrying spores of the fungus Ceratocystis novo ulmi Brasier, which causes the elm tree disease, a serious threat to survival of these trees [9]. In this study, 22 novel Tem analogous with the general formula of $(R)_2P(O)–X–P(O)(R)_2$, (X = $NH(C_6H_4)_2NH$, $NH(C_6H_4)SO_2(C_6H_4)NH$, $NH(C_6H_4)O(C_6H_4)NH$; R=(NC_4H_8O, NC_5H_{10}, NC_6H_{12}, OC_6H_5, C_6H_5, $N(C_2H_5)_2$, OCH_3, OCH_2CH_3, NC_4H_9, NC_3H_8) (**1–22**) were synthesized and characterized by ^{31}P, ^{13}C, ^{1}H NMR and IR spectroscopy. The solid-state structures of $(NC_4H_8O)_2(O)PNH(C_6H_4)_2NHP(O)(NC_4H_8O)_2$ (**1**) and $(CH_3O)_2P(O)NH(C_6H_4)_2NHP(O)(OCH_3)_2$ (**7**) were determined by X-ray crystallography and used as reference for quantum mechanical (QM) calculations at B3LYP level. The activity of Tem derivatives on AChE was determined using a modified Ellman's method [10]. QSAR analyses were used to find the most efficient parameters to introduce a better mechanism of interaction between the selected molecules and the receptor site of human AChE. The insects *Xanthogaleruca luteola Müll* were collected from elm trees leaves and reared on leaves of Ulmus densa Litw. Same-aged larvae (third instars) were randomly selected for the bioassay.

Materials and methods

Instrument and calculations

The enzyme AChE (human erythrocyte; Sigma, Cat. No. C0663), AChE (insect, EC 3.1.1.7), Triton X-100, bovine serum albumin, alpha-naphthyl acetate, beta-naphthyl acetate, fast blue RR, DMSO and sodium dodecyl sulfate (SDS) were all from Sigma-Aldrich. Acetylthiocholine iodide (ATCh, 99 %, FLUKA), 5, 5′-dithiobis (2-nitrobenzoic acid) (DTNB, 98 %, Merck), Na_2HPO_4, NaH_2PO_4 (99 %) were used as supplied. ^{1}H, ^{13}C and ^{31}P spectra were recorded on a Bruker Avance DRX 250, 300 and 500 spectrometers. ^{1}H and ^{13}C chemical shifts were determined relative to internal TMS, and ^{31}P chemical shifts were determined relative to 85 % H_3PO_4 as the external standard. Infrared (IR) spectra were recorded on a Shimadzu model IR-60 spectrometer using KBr pellets. Melting points of the compounds were obtained with an electrothermal instrument. UV spectrophotometer was operated using a PerkinElmer Lambda 25. Differential scanning calorimetry (DSC) was performed on a Du Pont® 910 Calorimeter, controlled by a 1090 Thermal Analyzer System. The insecticide and anti-AChE activities of these compounds were predicted by the Prediction of Activity Spectrum for Substances (PASS) software (version 1.193) [11]. The correlation analysis was performed by the Statistical Package for Social Scientists (SPSS) version 16.0 for Windows [12]. X-ray data of compounds **1** and **7** were collected on a Bruker SMART 1000 CCD area detector with graphite monochromated Mo-$K\alpha$ radiation (λ = 0.71073 Å) and refined by full-matrix least squares methods against F^2 with *SHELXL97* [13].

General synthesis

Compounds **1–22** were prepared by the reaction of a solution of diamine (1 mmol), and triethylamine (2 mmol) in CH_3CN was added at 0 °C to a solution of $Cl_3P(O)$ (2 mmol) in CH_3CN. After 3- to 5-h stirring, it was filtered and the some varied amine was added to solution. After 6 h in −5 °C, it was filtered and powder washed with distilled water and ethanol. The synthesis pathway of compounds is represented in Scheme 1.

*$(NC_4H_8O)_2(O)P–NH(C_6H_4)_2NH–P(O)(NC_4H_8O)_2$ (**1**)*

Powder sample; m.p. 187 °C. $^{31}P\{^{1}H\}$ NMR (DMSO-d_6, 298 K); δ = 10.35 (m) ppm. ^{1}H NMR (DMSO-d_6, 298 K); δ = 3.02 (m, 16 H, CH_2), 3.47 (m, 16 H, CH_2), 7.17 (d, $^{3}J_{(H–H)ben}$ = 8.45, 4 H, Ar–H), 7.30 (d, $^{2}J_{(PNH)}$ = 9.55, 2 H, NH_{ben}), 7.43 (d, $^{3}J_{(H–H)ben}$ = 8.45, 4 H, Ar–H) ppm. ^{13}C NMR (DMSO-d_6, 298 K); δ = 44.8 (s, CH_2), 66.9 (d, $^{3}J_{(P,C)mor}$ = 5.86 Hz, CH_2), 118.6 (d, $^{3}J_{(P,C)ben}$ = 6.74 Hz, CH), 126.6 (s, CH), 132.4 (s, C), 141.5 (s, C) ppm. IR (KBr, cm^{-1}): $\tilde{\upsilon}$ = 3139.26 (NH), 2953, 2851, 1612, 1500, 1264, 1195 (P=O), 1114, 968 (P–N), 827, 726, 683, 507.

*$(NC_5H_{10})_2(O)P–NH(C_6H_4)_2NH–P(O)(NC_5H_{10})_2$ (**2**)*

Powder sample; m.p. 190 °C. $^{31}P\{^{1}H\}$ NMR (DMSO-d_6, 298 K); δ = 11.48 (m) ppm. ^{1}H NMR (DMSO-d_6, 298 K); δ = 1.38-1.63 (m, 24 H, CH_2), 2.98 (m, 16 H, CH_2), 7.02 (d, $^{2}J_{(PNH)}$ = 9.7 Hz, 2 H, NH_{ben}), 7.15 (d, $^{3}J_{(H–H)ben}$ = 8.30 Hz, 4 H, Ar–H), 7.39 (d, $^{3}J_{(H–H)ben}$ = 8.35 Hz, 4H, Ar–H) ppm. ^{13}C NMR (DMSO-d_6, 298 K); δ = 24.5 (s, CH_2), 26.3 (d, $^{3}J_{(P,C)py}$ = 4.71 Hz, CH_2), 45.4 (s, CH_2), 118.3 (s, CH), 126.3 (s, CH), 131.9 (s, C), 142.0 (s, C). IR (KBr, cm^{-1}): $\tilde{\upsilon}$ = 3425, 3185 (NH), 2929, 2848, 1613, 1498, 1376, 1210 (P=O)1113, 1069, 955 (P–N), 826, 722, 557.

*$(NC_6H_{12})_2(O)P–NH(C_6H_4)_2NH–P(O)(NC_6H_{12})_2$ (**3**)*

Powder sample; m.p. 175 °C. $^{31}P\{^{1}H\}$ NMR (DMSO-d_6, 298 K); δ = 13.71 (m) ppm. ^{1}H NMR (DMSO-d_6, 298 K); δ = 1.48-1.53 (m, 32 H, CH_2), 3.06 (m, 16 H, CH_2), 6.98 (d, $^{2}J_{(PNH)}$ = 9.13 Hz, 2 H, NH_{ben}), 7.21 (d, $^{3}J_{(H–H)ben}$ = 8.40 Hz, 4 H, Ar–H), 7.39 (d, $^{3}J_{(H–H)ben}$ = 8.35 Hz, 4 H, Ar–H) ppm. ^{13}C NMR (DMSO-d_6, 298 K); δ = 26.1(s,

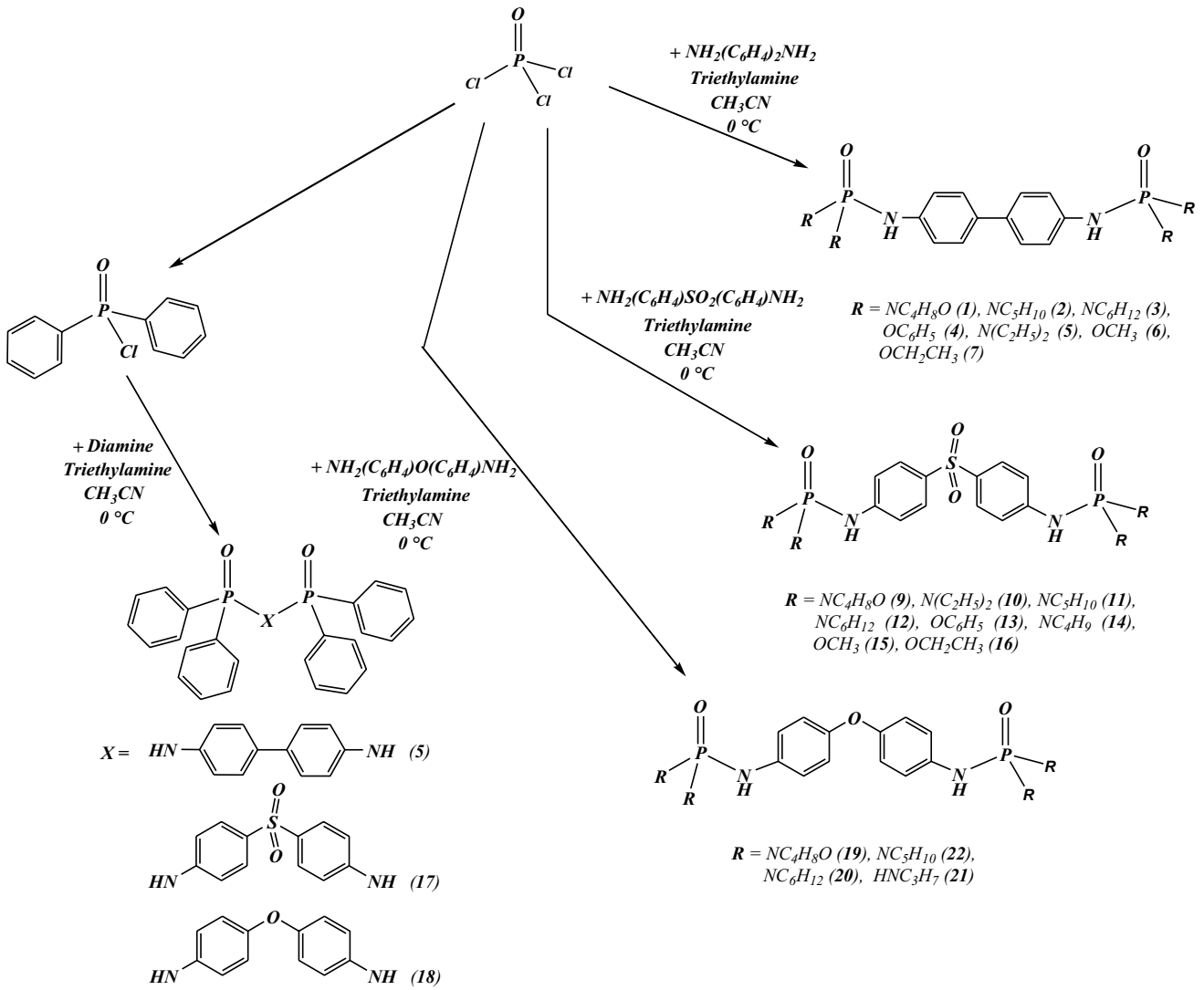

Scheme 1 The pathway of Temephos derivatives

CH_2), 29.8 (d, $^3J_{(P,C)hexa}$ = 3.77 Hz, CH_2), 47.0 (d, $^2J_{(P,C)hexa}$ = 3.72 Hz,CH2), 117.2 (d, $^3J_{(P,C)ben}$ = 6.66 Hz,CH), 127.9 (s, CH), 132.1 (s, C), 148.2 (s, C) ppm. IR (KBr, cm^{-1}): $\tilde{\upsilon}$ = 3410, 3208 (NH), 2924, 2854, 1613, 1497, 1380, 1190 (P=O), 1113, 1058, 931 (P–N), 825, 703, 526.

*$(OC_6H_5)_2(O)P{-}NH(C_6H_4)_2NH{-}P(O)(OC_6H_5)_2$ (**4**)*

Powder sample, m.p. 251 °C. $^{31}P\{^1H\}$ NMR (DMSO-d_6, 298 K); $\delta = -6.69$ (d) ppm. ^1H NMR (DMSO-d_6, 298 K); $\delta = 7.07$ (t, 4 H, CH, Ar–H), 7.28 (d, 8 H, CH, Ar–H), 7.17 (t, 8 H, Ar–H), 8.82 (d, 2 H, $^2J_{(PNH)}$ = 22.9 Hz, NH_{ben}) ppm. ^{13}C NMR (DMSO-d_6, 298 K); δ = 118.6 (d, $^3J_{(P,C)ben}$ = 7.81 Hz, CH), 120.4 (d, $^3J_{(P,C)oph}$ = 4.59 Hz, CH), 125.7 (s, CH), 127.5 (s, C), 130.4 (s, CH). 133.5 (s, CH), 139.2 (s, C), 150.5 (d, $^2J_{(POC)}$ = 6.31 Hz, C_{ipso}) ppm. IR (KBr, cm^{-1}): $\tilde{\upsilon}$ = 3142 (NH), 3054, 2947, 1611, 1589, 1490, 1398, 1321, 1264, 1231, 1184 (P=O), 1070, 1031, 1006, 982 (P–N), 948, 824, 752, 683, 567, 518, 484.

*$(C_6H_5)_2(O)P{-}NH(C_6H_4)_2NH{-}P(O)(C_6H_5)_2$ (**5**)*

Powder sample; m.p. 280 °C. $^{31}P\{^1H\}$ NMR (DMSO-d_6, 298 K); δ = 16.36 (s, $^2J_{(P,H)}$ = 11.35 Hz) ppm. ^1H NMR (DMSO-d_6, 298 K); δ = 7.07 (m, 16 H, CH), 7.28 (m, 8 H, CH, Ar–H), 7.17 (d, 4 H, Ar–H), 8.28 (s, 2 H, $^2J_{(P,H)}$ = 11.35 Hz, NH_{ben}) ppm. ^{13}C NMR (DMSO-d_6, 298 K); δ = 117.76 (s, Ar), 118.47 (m, CH), 120.48 (s, CH), 126.17 (s, CH), 126.63 (s, Ar), 128.23 (s, C), 128.51 (s, CH). 128.71 (s, Ar), 130.86 (s, Ar), 133.83 (s, CH), 140.71 (s, C), 150.5 (m, C_{ipso}), 151.26 (s, C) ppm. IR (KBr, cm^{-1}): $\tilde{\upsilon}$ = 3378 (NH), 3170, 2850, 1612, 1498, 1441, 1386, 1269, 1185 (P=O), 1117, 928 (P–N), 819, 724, 695, 527.

*$(N(C_2H_5)_2)_2(O)P-NH(C_6H_4)_2NH-P(O)(N(C_2H_5)_2)_2$ (**6**)*

Powder sample; m.p. 196 °C. $^{31}P\{^1H\}$ NMR (DMSO-d_6, 298 K); $\delta = 14.04$ (m) ppm. ^1H NMR (DMSO-d_6, 298 K); $\delta = 1.00$ (t, 24 H, CH_3), 2.98 (m, 16 H, CH_2), 6.88 (d, 2 H, $^2J_{(PNH)} = 8.85$ Hz, $NH_{2\text{-ben}}$), 7.18 (d, 4 H, $^3J_{(H-H)ben} = 7.4$, Ar–H), 7.37 (d, 4 H, $^3J_{(H-H)ben} = 7.40$, Ar–H) ppm. ^{13}C NMR (DMSO-d_6, 298 K); $\delta = 11.55$ (s, CH_3), 14.57 (d, $^2J_{(PNC)diet} = 1.53$ Hz, CH_2), 118.4 (d, $^3J_{(P,C)} = 6.57$ Hz, CH), 126.2 (s, CH), 131.9 (s, C), 142.3 (s, C) ppm. IR (KBr, cm^{-1}): $\tilde{\upsilon} = 3184$ (NH), 2972, 2876, 1614, 1498, 1464, 1380, 1209, 1175 (P=O), 1026, 940 (P–N), 823, 793, 711, 663, 529.

*$(OCH_3)_2(O)P-NH(C_6H_4)_2NH-P(O)(OCH_3)_2$ (**7**)*

Powder sample; m.p. 190 °C. $^{31}P\{^1H\}$ NMR (DMSO-d_6, 298 K); $\delta = 5.28$ (m) ppm. ^1H NMR (DMSO-d_6, 298 K); $\delta = 3.59$ (d, 12 H, $^3J_{(P,H)} = 11.03$ Hz, CH_3), 7.03 (d, 4 H, $^3J_{(H-H)ben} = 8.35$ Hz, Ar–H), 7.44 (d, 4 H, $^3J_{(H-H)ben} = 8.4$ Hz, Ar–H), 8.12 (d, 2 H, $^2J_{(PNH)} = 9.25$ Hz, $NH_{2\text{-ben}}$) ppm. ^{13}C NMR (DMSO-d_6, 298 K); $\delta = 53.29$ (s, CH_3), 118.0 (d, $^3J_{(P,C)} = 7.37$ Hz, CH), 127.1 (s, CH), 133.0 (s, C), 140.0 (s, C) ppm. IR (KBr, cm^{-1}): $\tilde{\upsilon} = 3150$ (NH), 2947, 2856, 1614, 1502, 1317, 1228 (P=O), 1043, 966 (P–N), 836, 753, 645, 597, 535.

*$(OCH_2CH_3)_2(O)P-NH(C_6H_4)_2NH-P(O)(OCH_2CH_3)_2$ (**8**)*

Powder sample; m.p. 168 °C. $^{31}P\{^1H\}$ NMR (DMSO-d_6, 298 K); $\delta = 2.41$ (m) ppm. ^1H NMR (DMSO-d_6, 298 K); $\delta = 1.22$ (t, 12 H, CH_3), 4.02 (m, 8 H, CH_2), 7.04 (d, 4 H, $^3J_{(H-H)ben} = 7.9$ Hz, Ar–H), 7.44 (d, 4 H, $^3J_{(H-H)ben} = 7.9$ Hz, Ar–H), 8.01 (d, 2 H, $^2J_{(PNH)} = 8.9$ Hz, $NH_{2\text{-ben}}$) ppm. ^{13}C NMR (DMSO-d_6, 298 K); $\delta = 16.49$(d, $^3J_{(P,C)} = 6.52$ Hz, CH_3), 62.4 (d, $^2J_{(P,C)} = 4.98$ Hz, CH_2), 118.00 (d, $^3J_{(P,C)ben} = 7.52$ Hz, CH), 126.98 (s, CH), 132.82 (s, C), 140.28 (s, C) ppm. IR (KBr, cm^{-1}): $\tilde{\upsilon} = 3191$ (NH), 3043, 2981, 1614, 1501, 1396, 1220 (P=O), 1026, 972 (P–N), 823, 745, 646, 523.

*$(NC_4H_8O)_2(O)P-NH(C_6H_4)SO_2(C_6H_4)NH-P(O)(NC_4H_8O)_2$ (**9**)*

Powder sample; m.p. 263 °C. $^{31}P\{^1H\}$ NMR (DMSO-d_6, 298 K); $\delta = 9.83$ (s) ppm. ^1H NMR (DMSO-d_6, 298 K): $\delta = 3.00$ (m, 16 H, CH_2), 3.45 (m, 16 H,CH_2), 7.23 (d, $^3J_{(H-H)Sulf} = 8.6$ Hz, 4H, Ar–H), 7.70 (d, $^3J_{(H-H)Sulf} = 8.6$, 4H, Ar–H), 7.83 (d, $^2J_{(PNH)Sulf} = 9.5$, 2 H, NH_{Sulf}) ppm. ^{13}C NMR (DMSO-d_6, 298 K); $\delta = 44.23$ (s, CH_2), 66.38 (d, $^3J_{(P,C)mor} = 5.7$ Hz, CH_2), 117.46 (d, $^3J_{(P,C)sulf} = 6.7$ Hz, CH), 128.35 (s, CH), 132.67 (s, C), 147.38 (s, C) ppm. IR (KBr, cm^{-1}): $\tilde{\upsilon} = 3403$ (N–H), 3141, 2851, 1594, 1496, 1303 (SO_2), 1257, 1195 (P=O), 1111 (SO_2), 968 (P–N), 923, 837, 698, 587.

*$(N(C_2H_5)_2)_2(O)P-NH(C_6H_4)SO_2(C_6H_4)NH-P(O)(N(C_2H_5)_2)_2$ (**10**)*

Powder sample; m.p. 193 °C. $^{31}P\{^1H\}$ NMR (DMSO-d_6, 298 K); $\delta = 13.61$ (m) and 15.33 (s) ppm. ^1H NMR (DMSO-d_6, 298 K); $\delta = 0.95$ (m, 24 H, CH_3), 2.97 (m, 16 H,CH_2), 7.29 (d, $^3J_{(H-H)Sulf} = 8.7$ Hz, 4 H, Ar–H), 7.51 (d, $^2J_{(PNH)Sulf} = 9.0$ Hz, 2 H, NH_{Sulf}), 7.61 (d, $^3J_{(H-H)Sulf} = 8.7$ Hz, 4 H, Ar–H). ^{13}C NMR (DMSO-d_6, 298 K); $\delta = 14.13$ (m, CH_3), 41.20 (s, CH_2), 117.19 (d, $^3J_{(P,C)Sulf} = 6.2$ Hz, CH), 128.08 (s, CH), 132.14 (s, C), 148.21 (s, C) ppm. IR (KBr, cm^{-1}): $\tilde{\upsilon} = 3323$ (N–H), 3189, 2973, 2874, 1594, 1498, 1467, 1382, 1300 (SO_2), 1214, 1178 (P=O), 1150 (SO_2), 1104, 1028, 945 (P–N), 910, 838, 792, 665, 578.

*$(NC_5H_{10})_2(O)P-NH(C_6H_4)SO_2(C_6H_4)NH-P(O)(NC_5H_{10})_2$ (**11**)*

Powder sample; m.p. 243 °C. $^{31}P\{^1H\}$ NMR (DMSO-d_6, 298 K); $\delta = 11.03$ (s) ppm. ^1H NMR (DMSO-d_6, 298 K); $\delta = 1.42$ (m, 24 H, CH_2), 2.95 (m, 16 H, CH_2), 7.26 (d, $^3J_{(H-H)Sulf} = 8.3$ Hz, 4 H, Ar–H),7.63 (d, $^2J_{(PNH)Sulf} = 9.1$ Hz, 2 H, NH_{Sulf}), 7.65 (d, $^3J_{(H-H)Sulf} = 8.3$ Hz, 4 H, Ar–H).^{13}C NMR (DMSO-d_6, 298 K); $\delta = 24.5$ (s, CH_2), 26.3 (d, $^3J_{(P,C)py} = 4.7$ Hz, CH_2), 45.4 (s, CH_2), 118.3 (s, CH), 126.3 (s, CH), 131.9 (s, C), 142.0 (s, C) ppm. IR (KBr, cm^{-1}): $\tilde{\upsilon} = 3182$ (N–H), 2931, 2847, 1593, 1496, 1378, 1301 (SO_2), 1209 (P=O), 1151 (SO_2), 1107, 1068, 955 (P–N), 916, 840, 686, 583.

*$(NC_6H_{12})_2(O)P-NH(C_6H_4)SO_2(C_6H_4)NH-P(O)(NC_6H_{12})_2$ (**12**)*

Powder sample; m.p. 250 °C. $^{31}P\{^1H\}$ NMR (DMSO-d_6, 298 K); $\delta = 13.45$ (m) ppm. ^1H NMR (DMSO-d_6, 298 K); $\delta = 1.46$ (m, 32 H, CH_2), 3.02 (m, 16 H, CH_2), 7.32 (d, $^3J_{(H-H)Sulf} = 8.5$ Hz, 4 H, Ar–H), 7.58 (d, $^2J_{(PNH)Sulf} = 13.0$ Hz, 2 H, NH_{Sulf}), 7.62 (d, $^3J_{(H-H)Sulf} = 8.5$ Hz, 4H, Ar–H) ppm. ^{13}C NMR (DMSO-d_6, 298 K); $\delta = 26.1$ (s, CH_2), 29.8 (d, $^3J_{(P,C)hexa} = 3.7$ Hz, CH_2), 47.0 (d, $^2J_{(P,C)hexa} = 3.7$ Hz,CH_2), 117.2 (d, $^3J_{(P,C)Sulf} = 6.6$ Hz, CH), 127.9 (s, CH), 132.1 (s, C), 148.2 (s, C) ppm. IR (KBr, cm^{-1}): $\tilde{\upsilon} = 3147$ (NH), 2926, 2855, 1593, 1496, 1463, 1381, 1301 (SO_2), 1232, 1185 (P=O), 1151 (SO_2), 1106, 1059, 1004, 909 (P–N), 840, 686, 582.

*$(OC_6H_5)_2(O)P-NH(C_6H_4)SO_2(C_6H_4)NH-P(O)(OC_6H_5)_2$ (**13**)*

Powder sample; m.p. 287 °C. $^{31}P\{^1H\}$ NMR (DMSO-d_6, 298 K); $\delta = -7.74$ (s) ppm. ^1H NMR (DMSO-d_6, 298 K); $\delta = 1.90$ (d, $^3J_{(H-H)Sulf} = 9.2$ Hz, 4 H, Ar–H), 7.09 (d,

12 H, CH, Ar–H), 7.36 (d, 8 H, Ar–H), 7.82 (d, $^3J_{(H–H)Sulf}$ = 9.2 Hz, 4 H, Ar–H), 9.5 (m, 2 H, NH_{Sulf}) ppm. ^{13}C NMR (DMSO-d_6, 298 K): δ = 118.6 (d, $^3J_{(P,C)Sulf}$ = 7.8 Hz, CH), 120.4 (d, $^3J_{(P,C)oph}$ = 4.5 Hz, CH), 125.7 (s, CH), 127.5 (s, C), 130.4 (s, CH), 133.5 (s, CH), 139.2 (s, C), 150.5 (d, $^2J_{(POC)}$ = 6.3 Hz, C_{ipso}) ppm. IR (KBr, cm^{-1}): $\tilde{\upsilon}$ = 3149 (N–H), 3058, 2944, 1593, 1490, 1392, 1301 (SO_2), 1189 (P=O), 1152 (SO_2), 1100, 951 (P–N), 833, 763, 687, 588, 512.

*$(NC_4H_9)_2(O)P–NH(C_6H_4)SO_2(C_6H_4)NH–P(O)(NC_4H_9)_2$ **(14)***

Powder sample; m.p. 243 °C. $^{31}P\{^1H\}$ NMR (DMSO-d_6, 298 K): δ = 2.45 (m) ppm. ^1H NMR (DMSO-d_6, 298 K); δ = 1.14 (s, 36 H, CH_3), 3.92 (d, 4 H, $^2J_{(PNH)amin}$ = 9.3 Hz, NH_{amin}), 7.18 (d, $^3J_{(H–H)Sulf}$ = 8.7 Hz, 4 H, Ar–H), 7.53 (d, 2 H, NH_{Sulf}), 7.58 (d, $^3J_{(H–H)Sulf}$ = 8.7 Hz, 4 H, Ar–H) ppm. ^{13}C NMR (DMSO-d_6, 298 K); δ = 13.16 (d, $^3J_{(P,C)amin}$ = 4.9 Hz, CH_3), 50.35 (s, C), 117.19 (d, $^3J_{(P,C)Sulf}$ = 6.2 Hz, CH), 128.08 (s, CH), 132.14 (s, C), 148.21 (s, C) ppm. IR (KBr, cm^{-1}): $\tilde{\upsilon}$ = 3370 (m, N–H), 2968, 1596, 150, 1384, 1304 (SO_2), 1224 (P=O), 1146 (SO_2), 1105, 1017, 912 (P–N), 840, 698, 587.

*$(OCH_3)_2(O)P–NH(C_6H_4)SO_2(C_6H_4)NH–P(O)(OCH_3)_2$ **(15)***

Powder sample; m.p. 170 °C. $^{31}P\{^1H\}$ NMR (DMSO-d_6, 298 K); δ = 3.88 (m) and 4.50 (s) ppm. ^1H NMR (DMSO-d_6, 298 K): δ = 3.63 (d, 12 H, $^3J_{(P,H)}$ = 4.3 Hz, CH_3), 7.13 (d, 4 H, $^3J_{(H–H)Sulf}$ = 8.2 Hz, Ar–H), 7.74 (d, 4 H, $^3J_{(H–H)Sulf}$ = 8.2 Hz, Ar–H), 8.71 (d, 2 H, $^2J_{(PNH)\ Sulf}$ = 8.7 Hz, NH_{Sulf}). ^{13}C NMR (DMSO-d_6, 298 K): δ = 53.29 (s, CH_3), 118.0 (d, $^3J_{(P,C)Sulf}$ = 7.3 Hz, CH), 127.1 (s, CH), 133.0 (s, C), 140.0 (s, C) ppm. IR (KBr, cm^{-1}): $\tilde{\upsilon}$ = 3147 (N–H), 3052, 2951, 1596, 1499, 1395, 1305 (SO_2), 1234 (P=O), 1150 (SO_2), 1107, 1038, 951 (P–N), 839, 755, 694, 579.

*$(OCH_2CH_3)_2(O)P–NH(C_6H_4)SO_2(C_6H_4)NH–P(O)(OCH_2CH_3)_2$ **(16)***

Powder sample; m.p. 188 °C. $^{31}P\{^1H\}$ NMR (DMSO-d_6, 298 K); δ = 0.99 (m) and 1.52 (s) ppm. ^1H NMR (DMSO-d_6, 298 K); δ = 1.18 (t, 12 H, CH_3), 3.98 (m, 8 H, CH_2), 7.13 (d, 4 H, $^3J_{(H–H)Sulf}$ = 5.9 Hz, Ar–H), 7.72 (d, 4 H, $^3J_{(H–H)Sulf}$ = 5.7 Hz, Ar–H), 8.62 (d, 2 H, $^2J_{(PNH)Sulf}$ = 7.6 Hz, NH_{Sulf}) ppm. ^{13}C NMR (DMSO-d_6, 298 K); δ = 16.49 (d, $^3J_{(P,C)}$ = 6.5 Hz, CH_3), 62.4 (d, $^2J_{(P,C)}$ = 4.9 Hz, CH_2), 118.00 (d, $^3J_{(P,C)Sulf}$ = 7.5 Hz, CH), 126.98 (s, CH), 132.82 (s, C), 140.28 (s, C) ppm. IR (KBr, cm^{-1}): $\tilde{\upsilon}$ = 3187 (N–H), 2982, 1596, 1501, 1395, 1305 (SO_2), 1230 (P=O), 1152 (SO_2), 1106, 1026, 970 (P–N), 832, 693, 584.

*$(C_6H_5)_2(O)P–NH(C_6H_4)SO_2(C_6H_4)NH–P(O)(C_6H_5)_2$ **(17)***

Powder sample; m.p. 272 °C. $^{31}P\{^1H\}$ NMR (MeOD-d_4, 300 K); δ = 21.55 (s) ppm. ^1H NMR (MeOD-d_4, 300 K): δ = 6.62 (d, $^3J_{(H–H)Sulf}$ = 8.7 Hz, 4 H, Ar–H), 7.10 (d, $^3J_{(H–H)Sulf}$ = 8.7 Hz, 4 H, Ar–H), 7.49 (m, 4 H, Ar–H), 7.59 (m, 8 H, Ar–H), 7.79 (m, 8 H, Ar–H) ppm. ^{13}C NMR (MeOD-d_4, 300 K); δ = 128.60 (s, C), 129.32 (d, $^2J_{(P,C)ph}$ = 7.3 Hz, CH), 130.01 (s, CH), 130.19 (s, C), 130.37 (d, $^3J_{(P,C)Sulf}$ = 7.8 Hz, CH), 132.93 (s, CH), 133.07 (s, CH), 133.90 (s, C) ppm. IR (KBr, cm^{-1}): $\tilde{\upsilon}$ = 3364 (N–H), 3106, 2925, 2854, 1710, 1593, 1496, 1438, 1392, 1298, 1248 (P=O), 1182, 1142 (SO_2), 1105, 923 (P–N), 834, 693, 583, 526.

*$(C_6H_5)_2(O)P–NH(C_6H_4)O(C_6H_4)NH–P(O)(C_6H_5)_2$ **(18)***

Powder sample; m.p. 97 °C. $^{31}P\{^1H\}$ NMR ($CDCl_3$, 300 K); δ = 19.03 (s) ppm. ^1H NMR ($CDCl_3$, 300 K); δ = 6.72 (m, 4 H, Ar–H), 7.10 (m, 4 H, Ar–H), 7.47 (m, 4 H, Ar–H), 7.69 (m, 8 H, Ar–H), 7.89 (m, 8 H, Ar–H) ppm. ^{13}C NMR (DMSO-d_4, 300 K); δ = 119.02 (m, CH), 119.73 (m, CH), 128.47 (m, CH), 128.74 (m, CH), 130.95 (d, $^2J_{(P,C)ph}$ = 2.79 Hz, CH), 131.69 (m, CH), 133.83 (s, C), 134.16 (s, C), 135.94 (s, C), 137.39 (s, C), 151.07 (s, C), 151.26 (s, C) ppm. IR (KBr, cm^{-1}): $\tilde{\upsilon}$ = 3385 (N–H), 3106, 3056, 2853, 1618, 1498, 1439, 1384, 1214, 1182 (P=O), 1120, 932 (P–N), 835, 696, 522.

*$(NC_4H_8O)_2(O)P–NH(C_6H_4)O(C_6H_4)NH–P(O)(NC_4H_8O)_2$ **(19)***

Powder sample; m.p. 135 °C. $^{31}P\{^1H\}$ NMR (DMSO, 300 K); δ = 10.75 (s) ppm. ^1H NMR ($CDCl_3$, 300 K); δ = 3.02 (d, 16 H, CH_2), 3.46 (d, $^3J_{(P,H)}$ = 4.1 Hz, 16 H, CH_2), 6.52 (d, $^3J_{(H–H)}$ = 8.1 Hz, 4 H, CH), 6.62 (d, $^3J_{(H–H)}$ = 8.1 Hz, 4 H, CH) ppm. ^{13}C NMR (DMSO-d_6, 300 K); δ = 42.60 (s, CH_2), 44.41 (s, CH_2), 63.23 (s, CH_2), 66.49 (d, $^3J_{(P,C)mor}$ = 5.8 Hz, CH_2), 115.11 (s, CH), 118.94 (s, CH), 143.55 (s, C), 148.63 (s, C) ppm. IR (KBr, cm^{-1}): $\tilde{\upsilon}$ = 3445 (N–H), 3224, 2961, 2854, 1621, 1500, 1217 (P=O), 1106, 967 (P–N), 840, 722, 601, 494.

*$(NC_6H_{12})_2(O)P–NH(C_6H_4)O(C_6H_4)NH–P(O)(NC_6H_{12})_2$ **(20)***

Powder sample; m.p. 178 °C. $^{31}P\{^1H\}$ NMR ($CDCl_3$, 300 K); δ = 14.65 (s) ppm. ^1H NMR ($CDCl_3$, 300 K); δ = 1.60 (m, 32 H, CH_2), 3.18 (m, 16 H, CH_2), 4.49 (m, 2 H, NH), 6.80 (m, 4 H, Ar–H), 7.06 (m, 4 H, Ar–H) ppm.

^{13}C NMR ($CDCl_3$, 300 K); $\delta = 24.83$ (s, CH_2), 26.41 (s, CH_2), 29.97 (d, $^3J_{(P,C)hexa} = 4.3$ Hz, CH_2), 45.22 (s, CH_2), 47.48 (s, CH_2), 115.77 (s, CH), 118.76 (m, C), 119.07 (s, C) ppm. IR (KBr, cm^{-1}): $\tilde{\upsilon} = 3203$ (NH), 2925, 2854, 1622, 1499, 1381, 1218, 1189 (P=O), 1112, 1058, 1004, 937 (P–N), 702, 512.

$(HNC_3H_7)_2(O)P-NH(C_6H_4)O(C_6H_4)NH-P(O)(HNC_3H_7)_2$ (21)

Powder sample; ^{31}P{^{1}H} NMR ($CDCl_3$, 300 K); $\delta = 7.50$ (s) ppm. ^{1}H NMR ($CDCl_3$, 300 K): $\delta = 1.14$ (m, 24 H, CH_3), 2.42 (m, 4 H, CH), 3.46 (d, $^2J_{(PNH)} = 13.0$, 2 H, NH), 5.11 (d, $^2J_{(PNH)} = 13.0$, 2 H, NH), 6.80 (d, $^3J_{(H-H)} = 8.5$ Hz, 4 H, Ar–H), 7.06 (d, $^3J_{(H-H)} = 8.5$ Hz, 4 H, Ar–H) ppm. ^{13}C NMR (DMSO-d_6, 300 K); $\delta = 25.13$ (m, CH_3), 42.32 (m, CH), 117.98 (s, Ar), 119.06 (s, Ar), 117.98-150.00 (Ar) ppm. IR (KBr, cm^{-1}): $\tilde{\upsilon} = 3224$ (NH), 2967, 2848, 1623, 1501, 1389, 1218, 1174 (P=O), 1033, 932 (P–N), 510.

$(NC_5H_{10})_2(O)P-NH(C_6H_4)O(C_6H_4)NH-P(O)(NC_5H_{10})_2$ (22)

Powder sample; m.p. 135 °C. ^{31}P{^{1}H} NMR ($CDCl_3$, 300 K): $\delta = 12.61$ (s) ppm. ^{1}H NMR (300.13 MHz, $CDCl_3$, 300 K): $\delta = 1.54$ (m, 24 H, CH_2), 3.06 (m, 16 H, CH_2), 6.64 (m, 4 H, Ar–H), 6.82 (m, 2 H, NH), 7.01(m, 4 H, Ar–H). ^{13}C NMR (DMSO-d_6, 300 K); $\delta = 21.88$ (s, CH_2), 22.16 (s, CH_2), 24.28 (s, CH_2), 25.88 (d, $^3J_{(P,C)py} = 4.8$ Hz, CH_2), 43.44 (s, CH_2), 44.93 (s, CH_2), 114.77 (s, CH), 118.76 (s, CH), 150.64 (s, C) 157.64 (s, C) ppm. IR (KBr, cm^{-1}): $\tilde{\upsilon} = 3182$ (N–H), 2931, 2847, 1593, 1496, 1378, 1301 (SO_2), 1209 (P=O), 1151, 1107, 1068, 955 (P–N), 916, 840, 686, 583.

Evaluation of biological activity

Human AChE assay

Human cholinesterase activity measurements were taken essentially according to the method of Ellman [10]. The reaction was carried out at 37 °C in 70 mM phosphate buffer (Na_2HPO_4/NaH_2PO_4, pH 7.4) containing the AChE enzyme (10-µl volume, diluted 100 times in phosphate buffer, pH 7.4), DTNB (5, 5′-dithiobis (2-nitrobenzoic acid)) (10^{-4} M concentration) and ATCh (1.35×10^{-4} M concentration). Each compound was dissolved in dimethyl sulfoxide (DMSO), which was then added to the buffer for in vitro cholinesterase assays. The highest concentration of DMSO used in the assays was 5 %. In the independent experiments without the inhibitor, 5 % DMSO had no effect on the inducing activity of the enzyme. The absorbance change at 37 °C was monitored with the spectrophotometer at 412 nm for 3 min, and three replicates were run in each experiment. In the absence of inhibitor, the absorbance change was directly proportional to the enzyme level. The reaction mixtures for determination of IC_{50} values (the median inhibitory concentration) consisted DTNB solution, 100 µl; inhibitor, x µl; acetylthiocholine iodide (ATCh) solution, 40 µl; phosphate buffer, $(850 - x)$ µl; and AChE solution, 10 µl. The activity of BChE was determined the same as the AChE activity by measuring the concentration of thiocholine, which reacted with DTNB after hydrolysis of BTCh. The lyophilized BChE was diluted with 100 mM phosphate buffer (pH 7.4) for using in the activity assay. The plot of V_I/V_0 (V_I and V_0 are the activity of the enzyme in the presence and absence of inhibitors, respectively) against log[I] (where, [I] is the inhibitor's concentration) gave the IC_{50} values of 16 compounds **1, 3**, **6–11**, **13–16**, **18–19** and **21–22** (as anti-AChE) (Table 1; Fig. 1).

Insect AChE assay

For sample preparation, adults were treated with different concentrations collected and transferred to a freezer (−20 °C). For measuring of enzyme activity, the sample was homogenized in cold double-distilled water using a hand-held glass homogenizer and centrifuged at 10,000 rpm for 10 min at 4 °C. After homogenization, they were centrifuged at 10,000 rpm for 15 min at 4 °C. AChE activity was determined at room temperature in 50 mM phosphate buffer (pH 7), 0.01 m DTNB and 0.01 m acetylthiocholine iodide stock solutions. Appropriate amounts of the substances were dissolved in phosphate buffer, pH 7, and these solutions were kept at 5 °C not longer than 2–3 days. The suitable working concentrations of DTNB and acetylthiocholine iodide were prepared immediately before use by dilution with buffer solution. The supernatant (40 µl) was added to a tube containing 140 µl of the buffer and 20 µl of DTNB and 40 µl ATCH. The concentration of reducing sugars obtained from the catalyzed reaction was measured by the method according to Elman [10]. Absorbance was measured at 412 nm. The sample was homogenized in 200 µl phosphate buffer. The homogenates were centrifuged at 12,000 g for 10 min at 4 °C. The supernatants as the enzyme source were pooled and stored at −20 °C for later use. For enzyme assay, 12.5 µl of supernatant was mixed with equal volume of substrates (6.4 mM alpha-naphthyl acetate or 6.4 mM beta-naphthyl acetate) and incubated at 30 °C for 3 min. Then, 50 µl of fast blue solution (0.07 % and SDS 5 %) was added and esterase activity was determined in a spectrophotometer at 405 and 454 nm, respectively (Table 1).

Table 1 Experimental, predication and external validation step of the biological activity of the BPAT compounds

Compound	Prediction (PASS)		Experimental		
	Anti-AChE	Insecticide	HAChE[a]	IAChE[b]	
			IC_{50}	Mortality (%) (5000 ppm)[a]	IC_{50}
$(NC_4H_8O)_2(O)P–NH(C_6H_4)_2NH–P(O)(NC_4H_8O)_2$ (**1**)	0.212	–	0.313	–	–
$(NC_5H_{10})_2(O)P–NH(C_6H_4)_2NH–P(O)(NC_5H_{10})_2$ (**2**)	0.257	–	–	–	–
$(NC_6H_{12})_2(O)P–NH(C_6H_4)_2NH–P(O)(NC_6H_{12})_2$ (**3**)	0.257	–	0.177	–	–
$(OC_6H_5)_2(O)P–NH(C_6H_4)_2NH–P(O)(OC_6H_5)_2$ (**4**)	0.551	0.538	–	–	–
$(C_6H_5)_2(O)P–NH(C_6H_4)_2NH–P(O)(C_6H_5)_2$ (**5**)	0.244	0.390	–	–	–
$(N(C_2H_5)_2)_2(O)P–NH(C_6H_4)_2NH–P(O)(N(C_2H_5)_2)_2$ (**6**)	0.311	0.192	0.510	–	–
$(OCH_3)_2(O)P–NH(C_6H_4)_2NH–P(O)(OCH_3)_2$ (**7**)	0.593	0.619	0.490	–	–
$(OCH_2CH_3)_2(O)P–NH(C_6H_4)_2NH–P(O)(OCH_2CH_3)_2$ (**8**)	0.529	0.506	0.860	–	–
$(NC_4H_8O)_2(O)P–NH(C_6H_4)SO_2(C_6H_4)NH–P(O)(NC_4H_8O)_2$ (**9**)	0.217	–	2.390	–	–
$(N(C_2H_5)_2)_2(O)P–NH(C_6H_4)SO_2(C_6H_4)NH–P(O)(N(C_2H_5)_2)_2$ (**10**)	0.299	–	0.150	–	–
$(NC_5H_{10})_2(O)P–NH(C_6H_4)SO_2(C_6H_4)NH–P(O)(NC_5H_{10})_2$ (**11**)	0.255	–	0.066	–	–
$(NC_6H_{12})_2(O)P–NH(C_6H_4)SO_2(C_6H_4)NH–P(O)(NC_6H_{12})_2$ (**12**)	0.255	–	–	–	–
$(OC_6H_5)_2(O)P–NH(C_6H_4)SO_2(C_6H_4)NH–P(O)(OC_6H_5)_2$ (**13**)	0.520	0.475	0.720	–	–
$(NC_4H_9)_2(O)P–NH(C_6H_4)SO_2(C_6H_4)NH–P(O)(NC_4H_9)_2$ (**14**)	0.307	–	0.240	–	–
$(OCH_3)_2(O)P–NH(C_6H_4)SO_2(C_6H_4)NH–P(O)(OCH_3)_2$ (**15**)	0.556	0.561	0.165	–	–
$(OCH_2CH_3)_2(O)P–NH(C_6H_4)SO_2(C_6H_4)NH–P(O)(OCH_2CH_3)_2$ (**16**)	0.501	0.446	0.019	–	–
$(C_6H_5)_2(O)P–NH(C_6H_4)SO_2(C_6H_4)NH–P(O)(C_6H_5)_2$ (**17**)	0.244	0.285	–	–	–
$(C_6H_5)_2(O)P–NH(C_6H_4)O(C_6H_4)NH–P(O)(C_6H_5)_2$ (**18**)	0.223	0.455	0.436	20	405
$(NC_4H_8O)_2(O)P–NH(C_6H_4)O(C_6H_4)NH–P(O)(NC_4H_8O)_2$ (**19**)	0.201	0.188	1.027	5	1125
$(NC_6H_{12})_2(O)P–NH(C_6H_4)O(C_6H_4)NH–P(O)(NC_6H_{12})_2$ (**20**)	0.241	0.234	–	0	3807
$(HNC_3H_7)_2(O)P–NH(C_6H_4)O(C_6H_4)NH–P(O)(HNC_3H_7)_2$ (**21**)	0.496	0.348	1.505	20	487
$(NC_5H_{10})_2(O)P–NH(C_6H_4)O(C_6H_4)NH–P(O)(NC_5H_{10})_2$ (**22**)	0.241	0.234	0.146	10	702

[a] Human AChE

[b] Insecticide AChE

Insecticide assay

Compounds **18**–**22** were dissolved in DMSO and diluted with water (1:3) to obtain series concentrations of 5000, 2500, 1250, 850 and 650 ppm. The insects *Xanthogaleruca luteola Müll* were collected from elm trees leaves in Guilan provinces of Iran and reared on leaves of Ulmus densa Litw. Same-aged larvae (third instars) were randomly selected for the bioassay. Third instars larvae were dipped on each solution for 30 s, then put them on fresh leave in conditioned room (23 ± 2 °C, 75 % RH) after that mortality was assessed after 24 h, and data were corrected and subjected to probit analysis (Table 1).

Crystal structure determination

A crystal suitable for X-ray crystallography was obtained from a mixture of CH_3CN at room temperature for compounds **1** and **7** (Figs. 2, 3). The solid-state structure as starting point was fully optimized by using DFT calculations in the gas phase. Whereas X-ray crystallography cannot determine accurately the position of hydrogen atoms, optimization of hydrogen atoms positions was performed to investigate the hydrogen bond characters in solid-state structures. The H atoms of N–H groups were objectively localized in the difference Fourier synthesis and refined in isotropic approximation. To achieve this goal, the solid-state structure of crystal was modeled as four clusters (Fig. 6). Other atoms were kept frozen during the optimization. Such computational justifications have also been used to describe well the geometry and electronic aspects of X-ray structure [14]. Taking into consideration the large number of atoms in the model cluster, all optimizations were performed at B3LYP/6-311+G** level. The NBO [15] analysis was performed to compare the electronic features of gas-phase structures of compound **7** with those of the model clusters at B3LYP/6-311+G** level [16]. As part of this study deals with investigation of the hydrogen bonds between O···H atoms, AIM analysis at the B3LYP/6-311+G** has much importance. Two hydrogen bonds with different lengths were observed in compound **7**. The hydrogen bonding energies have been calculated, on the basis

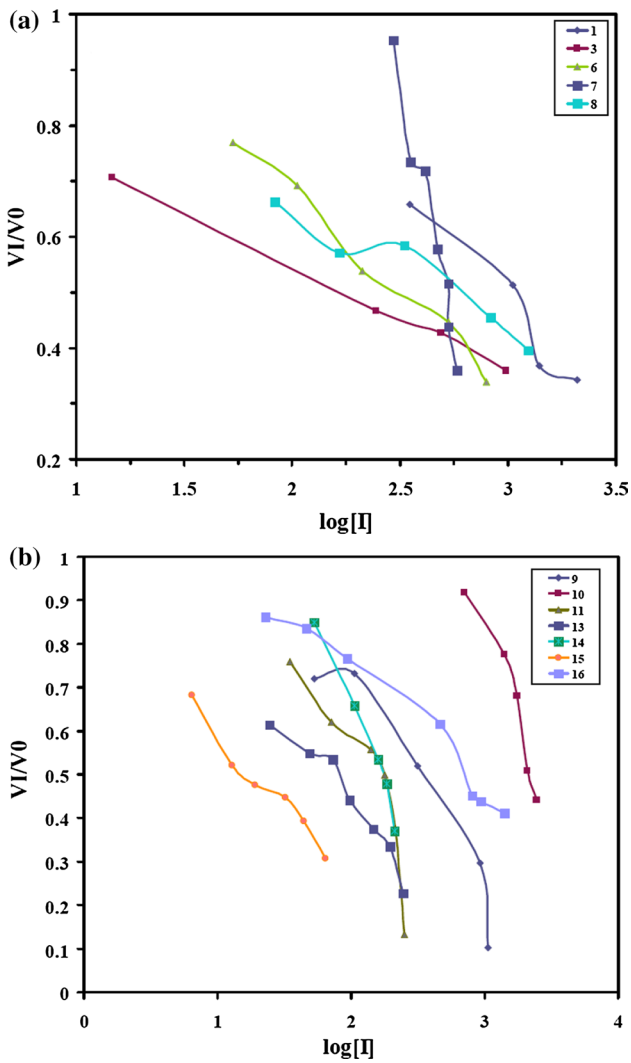

Fig. 1 Plot of V_I/V_0 against log[I] for inhibitors. V_I and V_0 are the AChE enzyme (A and B), activities (OD min^{-1}), and [I] is the inhibitor concentration (μM)

of energy difference between the hydrogen bonded dimmer and its monomers, as represented in equation $\Delta E_{HB} = (E_{dimer} - 2E_{monomer})/2$ and corrected for basis set superposition error (BSSE) using the counterpoise method [17]. All quantum chemical calculations were carried out by using the Gaussian 03 program package [18].

Statistical analysis

In order to identify the effect of physicochemical parameters on the AChE inhibition activity, QSAR studies were undertaken using the approach described by Hansch and Fujita [19]. The stepwise multiple linear regression procedure is a common method in QSAR studies for selection descriptors. The MLR method performed by the software package SPSS 16.0 was used for selection of the descriptors. The electronic and structural descriptors are obtained by either the quantum chemical calculations or theoretical and experimental studies. The electronic descriptors include the energy of frontier orbital (E_{HOMO} and E_{LUMO}), electrophilicity (ω), polarizability (PL, the charge difference between the atoms in functional groups) and the net atomic charges (Q). Also hydrophobic coefficient (log P), dipole moment (μ) and molecular volume (Mv) are the structural descriptors. E_{HOMO}, E_{LUMO}, ω, P, Q, μ and Mv values are obtained from the DFT results. The logarithm of partition coefficient (log P) is measured by the ChemDraw software. The toxicities of Tem analogous are expressed in terms of $\log(1/IC_{50})$ as an anti-cholinesterase activity. The descriptor values were related to toxicity using MLR analysis. MLR of descriptors, selected for biological activity, gives rise to the problem of multicollinearity. The descriptors with lower residuals and standard error ($S_{reg} < 0.5$) to $\log(1/IC_{50})$ were selected to carry out stepwise MLR analysis and to optimize the QSAR equation. The stable geometry structures of compounds were further fully optimized using the density functional theory (DFT) at the B3LYP/6-311+G** level of theory [20]. Statistical analysis of insecticide data was compared by one-way analysis of variance (ANOVA) followed by Tukey's test when significant differences were found at $P = 0.05$ using SAS program [21].

Results and discussion

Spectra study

The ^{31}P NMR chemical shift at room temperature in $CDCl_3$ and DMSO appears in the range −7.74 ppm (**13**) to 21.55 ppm (**17**). The ^{1}H NMR spectra of compounds **1**, **2**, **3**, **9**, **11–12**, **19**, **20** and **22** exhibited two signals for the methylene protons of the six-membered piperazinyl rings. Two protons of the NH group as two doublets are exhibited as a multiple peak at the range 4.49 ppm (**20**) to 9.50 ppm (**13**) and $^{2}J_{PNH} = 7.6$ Hz (**16**) to $^{2}J_{PNH} = 13.1$ Hz (**12**). The ^{13}C NMR spectra of compounds **1**, **2**, **3**, **9**, **11–12**, **19**, **20** and **22** indicated three separated peaks for the six carbon atoms that are due to different orientations of the aliphatic six-membered rings. The $^{3}J_{PC}$ have maximum value ($^{3}J_{PC} = 7.3$ Hz) in compound **17** arises from spin coupling of CH group carbon atom with phosphorus atom. The $^{3}J_{PC}$ values in titled compounds indicate that $^{3}J_{PC(aromatic)}$ are greater than $^{3}J_{PC(aliphatic)}$. The analysis of the IR spectra indicated that the fundamental ν(P=O) stretching modes for compounds **1–22** appeared at the range 1175–1234 cm^{-1}. Moreover, the N–H stretching frequencies for all compounds were observed at the range of 3139–3445 cm^{-1}.

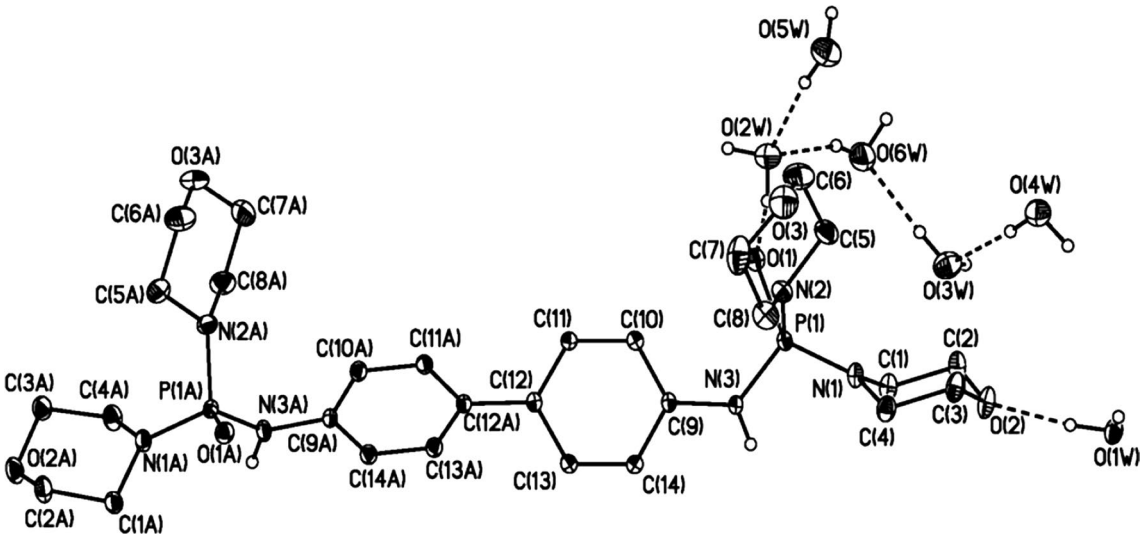

Fig. 2 ORTEP view of the first symmetrically independent molecule of **1**

Crystal structures

Single crystal of both compounds **1** and **7** suitable for X-ray diffraction analysis was grown from an acetonitrile solution after slow evaporation at room temperature. The crystal data and the details of X-ray analysis are given in Table 2; also molecular structures are shown in Figs. 2 and 3 for compounds **1** and **7**. Compound **1** crystallized in the monoclinic C 2/c space group. The phosphorus atom has a slightly distorted tetrahedral configuration in compound **1** that is the surrounding angles around the P atom are in the range of 104.85(6)°–115.67(5)°. The P=O bond distance is in **1** (1.4904(10) Å). The P–N bond distances in **1** (1.6384(11) Å), (1.6445(11) Å), (1.6552(11) Å) bond are shorter than the single bond P–N distance of 1.77 Å. The structure is not a traditional pillared material where the inorganic layer is linked by organic groups. Instead, the H_2O centers act as pillars that link organic layers together (Fig. 4). The asymmetric unit consists of four compound **1** sited on of symmetry with fourteen water molecule in the center and twenty-two of them in sides.

The thermogravimetric analysis is used to prove the existence of water in the composition **1**. The differential scanning calorimetry (DSC) curve of the dehydration of compound **1** (Fig. 5) shows that the dehydration occurs in the one step. Water molecules per structure unite is released in the temperature 278.83 °C. The crystal data and the details of the X-ray analysis of the compound **7** are given in Table 2. The phosphorus centers are in typical tetrahedral environments. The P=O bond lengths with the *anti*-configuration were observed for of 1.4708(10) Å for P(1)–O(1) and 1.4686(11) Å for P(1′)–O(1′), in $(CH_3O)_2P(O)NH(C_6H_4)–(C_6H_4)NHP(O)(OCH_3)_2$ (**7**). It seems that the difference in the bond lengths is correlated with the various orientations of benzene rings and OCH_3 groups. These orientations lead to the creation of different hydrogen bonding patterns between the P=O and N–H functional groups (Fig. 6). The one-dimensional polymeric chains form in the crystal lattice with cyclic $R_4^4(16)$ motifs in which the monomers are connected to each other via four P=O···H–N hydrogen bonds distance of 2.868(2) and 2.782(2) Å (Fig. 6, Table 3). The $R_Y^X(Z)$ graph–set notation is descriptive of a *Z*-membered ring produced by the *X* hydrogen bonds between the *Y* donor–acceptor units [22]. The low atomic radius and the large electronegativity of oxygen atoms increased the strength of the hydrogen bonding between P=O and NH. The electronic parameters of the hydrogen bonded clusters of compound **7** were calculated by AIM and NBO methods. The results of AIM and NBO analyses for the mentioned clusters are presented in Table 3. As shown, the bond lengths in this cluster are equal to those obtained from the X-ray structures, except for the C–H and N–H bonds, since the optimizations have been performed only for the hydrogen atoms' positions. Also the donor–acceptor distances for the hydrogen bonds in the model cluster are equal to the experimental values. The results of AIM analysis show that the electron density (ρ) value at the bond critical point (bcp) of O(1′)···H(1) (0.040 e $Å^{-3}$) bond path is larger in magnitude than the that calculated for the O(1)···H(1′) (0.031 e $Å^{-3}$) in the model cluster. The smaller ρ value at the bcp of N–H bond confirms the presence of the stronger hydrogen bonds in P(1′)–O(1′)···(1)H–N(1) with the linear N–H···O contact angle in comparison with the values obtained for P(1)–O(1)···(1′)H–N(1′). The ρ value at the bcp of N–H bonds is 0.332 e $Å^{-3}$ for the fully optimized structure in the gas phase, which decreases

Table 2 Crystallographic data of compounds

Forms	**1**	**7**
Empirical formula	C28H62N6O16P2	C36H30N2O6P2
Formula weight	800.78	648.56
Temperature (K)	100(2)	100(2)
Wavelength (Å)	0.71073	0.71073
Crystal system, space group	Monoclinic, C 2/c	Monoclinic, P 21/c
Unit cell dimensions		
a (Å)	19.4798(6)	8.2558(7)
b (Å)	26.3273(9)	33.787(3)
c (Å)	8.4918(3)	11.4912(10)
α (°)	90	90
β (°)	113.0160(10)	94.6057(19)
γ (°)	90	90
V (Å^3)	4008.3(2)	3195.0(5)
Z, calculated density (Mg m^{-3})	4	4
Density (calculated) (Mg/m^3)	1.327	1.348
Absorption coefficient (mm^{-1})	0.181	0.186
F(000)	1720	1.88°–29.00°
Crystal size (mm)	0.35 × 0.25 × 0.25 mm^3	0.40 × 0.15 x 0.14 mm^3
θ range for data collection (°)	2.27°–29.00°	1352
Limiting indices	$-26 \leq h \leq 26$	$-9 \leq h \leq 11$
	$-35 \leq k \leq 35$	$-46 \leq k \leq 43$
	$-11 \leq l \leq 11$	$-15 \leq l \leq 15$
Reflections collected/unique	24,387 5323 [R(int) = 0.0204]	25,961 8496 [R(int) = 0.0790]
Completeness to theta (%)	99.5	99.8
Absorption correction	Semiempirical from equivalents	Semiempirical from equivalents
Refinement method	Full-matrix least squares on F^2	Full-matrix least squares on F^2
Data/restraints/parameters	5323/0/236	5323/0/236
Goodness-of-fit on F^2	1.006	1.006
Final R indices	$R1 = 0.0409$, $wR2 = 0.1259$	$R1 = 0.0409$, $wR2 = 0.1259$
R indices (all data)	$R1 = 0.0457$, $wR2 = 0.1326$	$R1 = 0.0457$, $wR2 = 0.1326$
Largest diff. peak and hole (e Å^{-3})	0.943 and −0.351	0.943 and −0.351

to 0.308 and 0.312 e Å^{-3}, respectively, in N(1)–H(1) and N(1′)–H(1′). The mean N–H distance increases from the isolated molecules from 0.90 to 1.031 Å in their hydrogen bonded of the modeled cluster. The electronic delocalization of Lp(O)$_i$ → σ*(N–H)$_j$ occurs when the hydrogen bonds are formed between the subunits i and j within a cluster. Such an electronic effect leads to weakening of the N–H bond. It has been previously explained that the stabilizing energy E^2 increases by a decrease in the donor–acceptor distance of hydrogen bond [23]. The stabilizing energies E^2 of Lp(O)$_i$ → σ*(N–H)$_j$ electron density transfer in P=O···H–N hydrogen bonds in the model cluster have been calculated as 32.63 and 27.89 kJ mol^{-1}, respectively. This is in agreement with the values of distance for these hydrogen bonds in two P(1′)–O(1′)···(1)H–N(1) (2.782(2) Å) and P(1)–O(1)···(1′) H–N(1′) (2.868(2) Å) models. The hydrogen bonding energy in P(1′)–O(1′)···(1)H–N(1) model (–72.15 kJ mol^{-1}) is higher than the value calculated for P(1)–O(1)···(1′) H–N(1′) (–45.67 kJ mol^{-1}) (Table 3). It is noteworthy that the term E^2 refers to the stabilization energy of electronic delocalization between the donor–acceptor orbital and differs from the hydrogen bonding energy.

Prediction of insecticide potential

PASS software predicts 900 types of biological activities based on the structural formula. The default list of predictable biological activities (P_a) includes the main and side pharmacological effects, molecular mechanisms and specific toxicities. The PASS prediction results for a compound are presented as a list of activity names and probability activity (P_a) values. The P_a values are interpreted as: if $P_a > 0.7$, $0.5 < P_a < 0.7$, and $P_a < 0.5$, then the chance of finding this activity in the experiments is high, low and

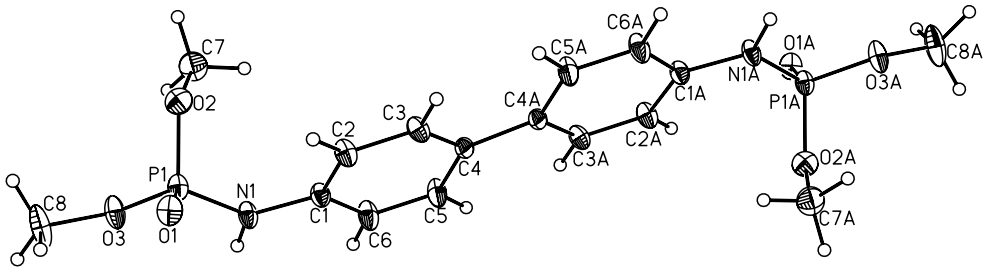

Fig. 3 ORTEP view of the first symmetrically independent molecule of **7**

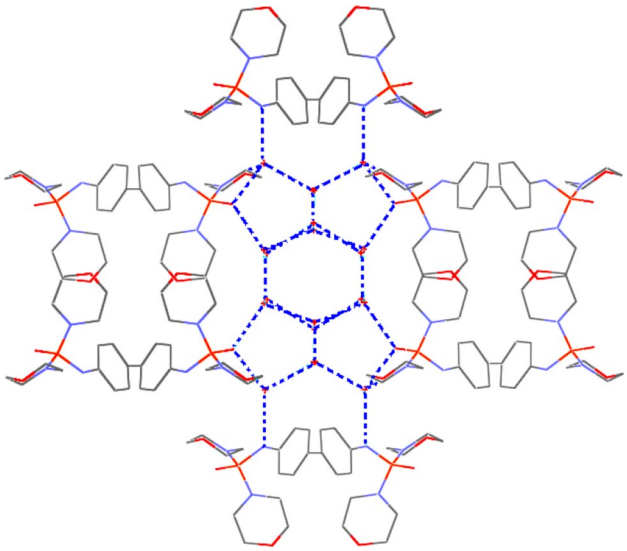

Fig. 4 Asymmetric unit consists of four compound **1** sited on of symmetry with fourteen water molecule in the center and twenty-two of them in sides

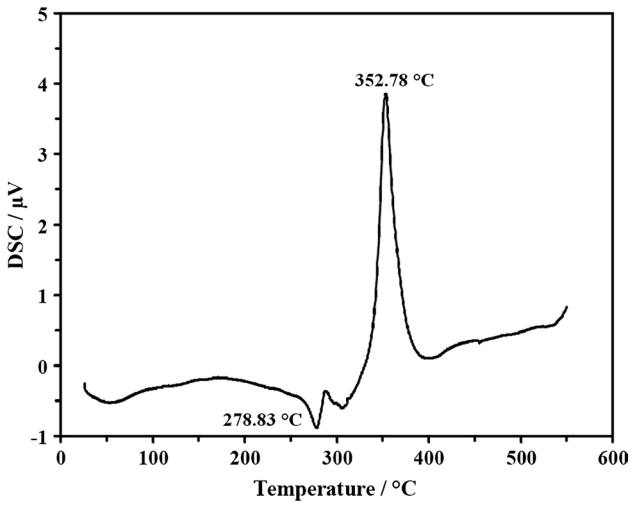

Fig. 5 DSC curve of compound **1**

lower, respectively [24]. Insecticide potential and anti-AChE activities of 23 Tem analogous have been obtained by using the PASS software, and the results are summarized in Table 1. The insecticidal properties of all compounds are predicted in the range of 0.188 (**19**) to 0.619 (**7**). As shown in Fig. 7a, a linear relationship gives the plot of probable insecticide potential against anti-AChE activity. To test the anti-AChE activity of the synthesized compounds, we evaluated the inhibitory potential of titled compounds against AChE enzyme by Ellman assay.

Bioassay

AChE assay

The inhibition constant (IC_{50}) values of AChE against compounds **1, 3**, **6–11**, **13–16**, **18–19** and **21–22** were in the range of 0.019 mM (**16**) to 2.390 (**9**) mM (Fig. 1a, b; Table 1). The comparison of experimental data (log(1/IC_{50}) and the prediction of anti-AChE activities are shown in Fig. 7b. In the terminal position of the compounds **1–8** with the $NH(C_6H_4)(C_6H_4)NH$ skeleton, cyclic aliphatic substitutions (NC_5H_{10}; IC_{50} = 0.313 mMol) inhibitory activity are higher than the non-cyclic aliphatic substitutions (NC_4H_{10}; IC_{50} = 0.510 mMol). The compound **16** with the $NH(C_6H_4)SO_2(C_6H_4)NH$ skeleton versus AChE displayed the most potent inhibitory activity. The inhibitory of compound **16** is higher than that of compound **13** with the $R_2(O)P–NH(C_6H_4)SO_2(C_6H_4)NH–P(O)R_2$ ($R=OC_2H_5$, OC_6H_5)., because the presence of the electron acceptor substituent in the around P=O group increases the inhibitory potential of Tem derivatives. The mixed-type and reversible mechanisms of Tem analogous were evaluated by Lineweaver–Burk plots in previous work [25]. To gain a better understanding of the inhibitory potential of the synthesized compounds and to study on the reversible mechanism in more detail, it was necessary to examine the interaction of the Tem derivatives with the AChE structures by QSAR method.

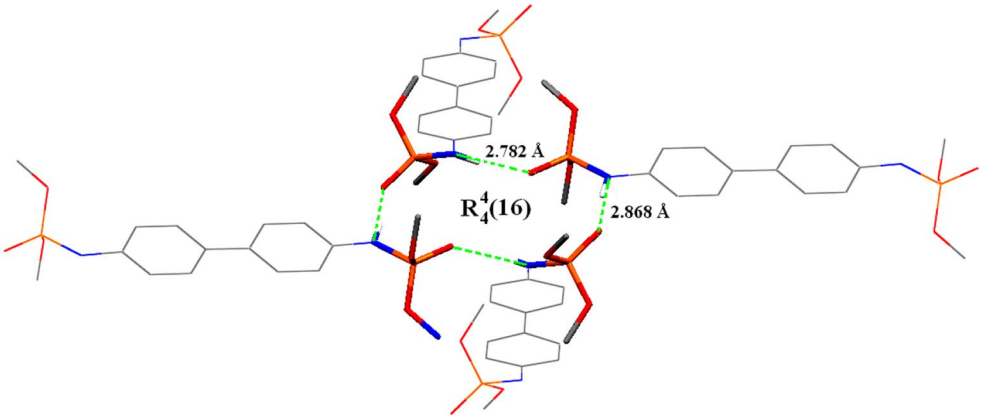

Fig. 6 Tetramer motifs $R_4^4(16)$ formed by four hydrogen bonds of P=O···H–N

Table 3 Hydrogen bonds data for the X-ray structure (the values in brackets), model cluster (at B3LYP/6-311+G**), charge densities (from AIM analysis), delocalization energy (from NBO analysis) and bonding energy (at B3LYP/6-311+G**) for the model cluster

D–H···A	d(N–H)	d(H···O)	d(N···O)	∠NHO	ρ at the b.c.p. (e Å^{-3})		$E^{(2)a}$	E^{b}_{HB}
					N–H	H···O		
N(1)–H(1)···O(1′)[c]	[1.031]0.90	[1.728]1.90	[2.782(2)]	[171.1]168.0	0.308	0.040	32.63	–72.15
N(1′)–H(1′)···O(1)[d]	[1.029]0.90	[1.844]1.98	[2.868(2)]	[172.3]169.0	0.312	0.031	27.89	–45.67
O(1W)–H(1WA)···O(1)[e]	0.83	1.97	2.7985(13)	174	–	–	–	–
O(1W)–H(1WB)···O(2)[f]	0.93	1.82	2.7472(15)	172	–	–	–	–
O(2W)–H(2WA)···O(5W)[g]	0.94	1.87	2.7938(18)	168	–	–	–	–
N(3)–H(3 N)···O(1W)[h]	0.84	2.20	3.0366(15)	176	–	–	–	–
O(2W)–H(2WB)···O(1)[f]	0.89	1.97	2.8599(14)	177	–	–	–	–
O(3W)–H(3WA)···O(6W)[f]	0.87	1.90	2.7683(17)	177	–	–	–	–
O(3W)–H(3WB)···O(1W)[i]	0.94	1.97	2.9117(17)	176	–	–	–	–
O(4W)–H(4WA)···O(3W)[f]	0.90	1.91	2.8139(15)	176	–	–	–	–
O(5W)–H(5WA)···O(2W)[f]	0.92	1.97	2.8847(17)	173	–	–	–	–
O(5W)–H(5WB)···O(4W)[j]	0.93	1.93	2.8531(16)	173	–	–	–	–
O(6W)–H(6WA)···O(2W)[f]	0.92	1.92	2.7924(15)	158	–	–	–	–

[a] The stabilizing energy E^2 refers to the effect of $Lp(O_P)_i \rightarrow \sigma^*(N–H)_j$ delocalization

[b] The binding energy in kJ mol^{-1} for N–H···S hydrogen bonds

[c] $-x+1, -y+1, -z+1$

[d] $x+1, y-1, z$

[e] $x, y, z+1$

[f] x, y, z

[g] $x, -y, z-1/2$

[h] $-x+1/2, -y+1/2, -z+3$

[i] $-x, y, -z+5/2$

[j] $-x, -y, -z+2$

Insecticide potential

Like the vertebrate AChEs, invertebrate AChEs belongs to α/ß hydrolase fold family, with a core of eight ß-sheets connected by α-helices [10]. The 3D structures of invertebrates are folded similarly, and their active sites closely overlap. The main structural differences between them are found in their external loops and in the tilt of the C-terminal helix, differences that are unlikely to affect catalytic function directly. The result of five monitoring showed that two compounds had the mortality effect nearly 20 % when we used the 5000-ppm concentration, in second section monitoring of compounds done, five of them selected for bioassay (Table 1). Also the amounts of IC_{50} for the enzyme of

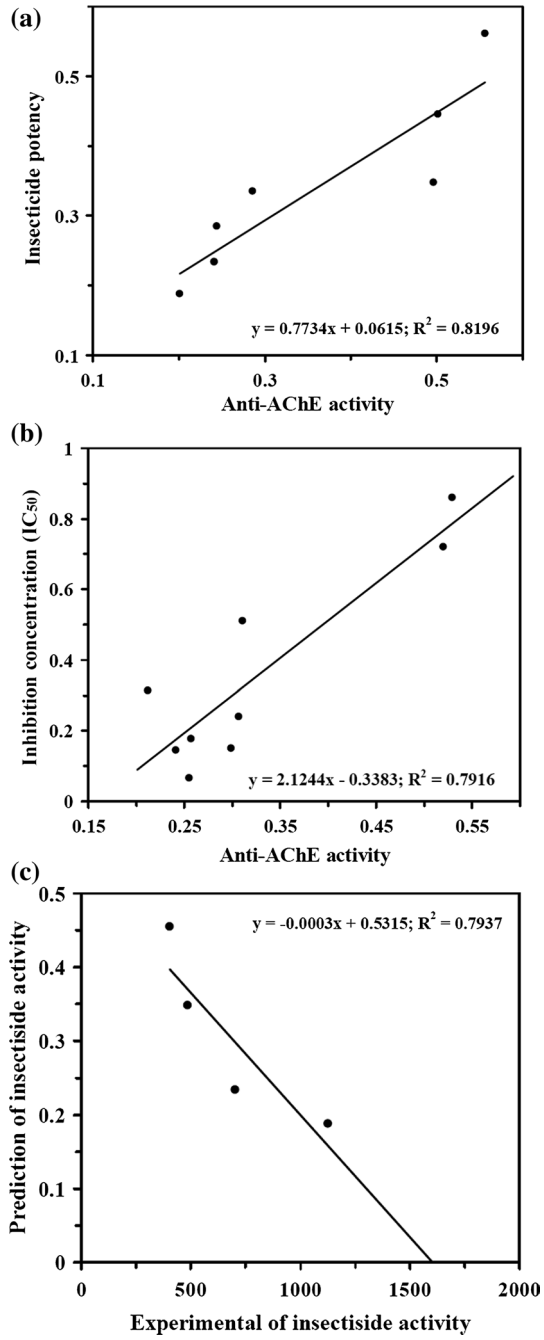

Fig. 7 Plot of probable insecticide potential against probable anti-AChE activity of selected compounds (**a**); the plot of experimental values against prediction of anti-AChE activity (**b**); the plot of probable insecticide potential against experimental insecticide potency (**c**)

human and insect treated with any compounds. Four concentrations 2500, 1250, 850 and 650 selected to apply the bioassay in third instars larvae of *X. luteola*. Our investigations demonstrate the compound of **18** had an insecticidal effect better than the other compounds, as the IC_{50} of it that was lesser. The high activity of compound **18** is depended to the increasing of concentration of inhibitor. Esterase is

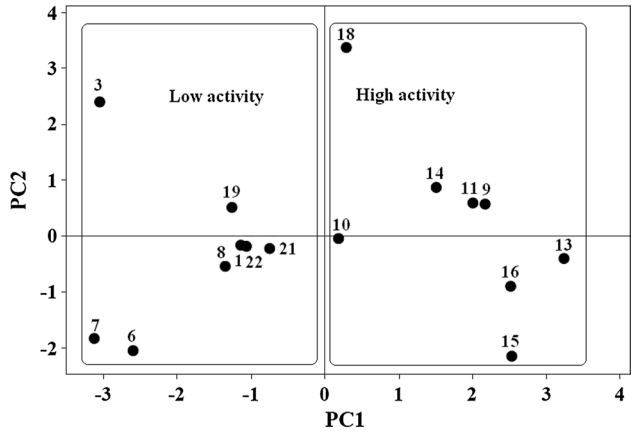

Fig. 8 PCA score plot for Tem derivatives

one of the important enzymes in insect. Most of them have a toxification role when the insects encounter to toxin compounds. As the alpha and beta esterase were measured from the treated larvae. The result showed compound **18** could inhibit α-esterase more than the other enzymes, because the AChE in most of insects belongs to this grope of esterase (Table 1). The comparison of experimental data and the prediction of insecticide activities are shown in Fig. 7c.

QSAR study

PCA-QSAR: PCA method was used to reduce the independent variables. The principal components (PCs) as a new set of variables (mutually orthogonal) were obtained by this method. The first PC contains the largest variance, and the second PC contains the second largest variance. The variable selection in PCA was performed by using the Fisher's weights approach [26], and the results are summarized as the following Eqs. (1a–1c):

$$\begin{aligned} PC_1 = &+0.172Q_P + 0.344Q_N - 0.251PL_{P=O} + 0.087PL_{N-H} \\ &- 0.456E_{HOMO} - 0.432E_{LUMO} + 0.431\omega \\ &+ 0.353\mu - 0.225\log P + 0.146Mv \end{aligned} \quad (1a)$$

$$\begin{aligned} PC_2 = &-0.586Q_P + 0.232Q_N + 0.450PL_{P=O} \\ &- 0.339PL_{N-H} + 0.099E_{HOMO} - 0.113E_{LUMO} \\ &+ 0.113\omega - 0.035\mu - 0.255\log P + 0.430Mv \end{aligned} \quad (1b)$$

$$\begin{aligned} PC_3 = &+0.200Q_P + 0.242Q_N - 0.375PL_{P=O} - 0.575PL_{N-H} \\ &- 0.078E_{HOMO} + 0.187E_{LUMO} - 0.169\omega \\ &- 0.026\mu + 0.414\log P + 0.434Mv \end{aligned} \quad (1c)$$

The main variables were found from the principle scores of the normalized eigenvalue of the three principal

Table 4 Quantum chemical and geometrical descriptors for the titled compounds computed at B3LYP/6-311+G** level

No.	Electronic descriptors							Structural descriptors		
	Charge		Polarizability		Frontier molecular orbital			Lipophilicity		Steric
	Q_P (a.u)	Q_N (a.u)	$PL_{P=O}$	PL_{N-H}	E_{HOMO}	E_{LUMO}	ω	μ (Debye)	log P	Mv (cm^3/mol)
1	2.337	−0.964	−3.499	1.389	−0.209	−0.038	0.089	6.98	−2.42	389.618
3	2.066	−0.965	−3.204	1.377	−0.204	−0.036	0.092	3.943	3.42	490.038
6	2.386	−0.996	−3.512	1.387	−0.204	−0.035	0.084	9.91	1.49	256.537
7	2.461	−0.986	−3.303	1.405	−0.206	−0.028	0.077	6.71	0.56	266.537
8	2.377	−0.964	−3.499	1.389	−0.211	−0.039	0.091	6.13	1.93	435.756
9	2.381	−0.950	−3.506	1.401	−0.233	−0.056	0.118	9.42	−4.23	520.925
10	2.390	−0.950	−3.520	1.380	−0.225	−0.036	0.090	12.19	−0.12	472.238
11	2.381	−0.945	−3.504	1.370	−0.231	−0.057	0.119	13.809	0.01	452.332
13	2.480	−0.963	−3.557	1.397	−0.244	−0.062	0.127	14.673	−2.90	511.893
14	2.351	−0.950	−3.488	1.378	−0.226	−0.052	0.106	14.03	−2.49	492.878
15	2.470	−0.950	−3.578	1.432	−0.238	−0.058	0.121	11.65	−1.24	314.121
16	2.469	−0.960	−3.577	1.380	−0.239	−0.059	0.123	16.03	−0.13	389.618
18	2.047	−0.964	−3.168	1.389	−0.213	−0.056	0.115	13.01	−6.80	442.067
19	2.363	−0.966	−3.440	1.376	−0.217	−0.035	0.087	5.70	−1.76	485.257
21	2.346	−0.968	−3.476	1.386	−0.213	−0.033	0.084	14.514	−2.23	408.458
22	2.377	−0.972	−3.509	1.395	−0.213	−0.033	0.084	9.70	−0.63	549.027

[a] Not tested due to insufficient quantities

components. The results showed the total variance of the first, second and third factor PC as 44.2, 21.4 and 12.8 %, respectively. Also, from the above equations, it was deduced that the frontier molecular orbital energy parameters (E_{HOMO}, E_{LUMO}, ω) in PC_1 are predominated from those related to electronic (Q_P, Q_N, $PL_{P=O}$ and PL_{N-H}) in PC_2 and structural parameters (log P and Mv) in PC_3 equation. Figure 8 shows the score and a loading plot of $PC_1 \times PC_2$. The score plot shows that separation of the compounds with $(NH(C_6H_4)_2NH$ and $NH(C_6H_4)O(C_6H_4)NH$ moieties (left side), and $NH(C_6H_4)SO_2(C_6H_4)NH$ moiety (right side) has been provided by PC_1. PC_1 equation was separated the compounds based on changing value of molecular orbital energy descriptors. For example, compounds **1–9** and **18–22** with the $E_{LUMO} = -0.028$ to -0.038 are in the right side of graph, whereas compounds **10–17** are in the left side (with the $E_{LUMO} = -0.052$ to -0.062). PCA-QSAR method cannot partially separated descriptors; it is just a total separation. The MLR-QSAR method can be used to solve this problem.

MLR-QSAR The stepwise MLR procedure which is a common method used in QSAR studies was used for model selection. The electronic and structural descriptors were obtained by quantum chemical calculations (Table 4). An optimal QSAR equation based on calculation data shown in Table 4 was obtained for 16 compounds as following:

$$\begin{aligned}\log(1/IC_{50}) &= +0.130\log P + 0.033\mu - 4.213Q_P - 8.915Q_N \\ &\quad - 0.317PL_{P=O} + 4.539PL_{N-H} - 64.050E_{HOMO} \\ &\quad - 64.143E_{LUMO} - 69.962\omega - 0.002Mv - 62.072 \\ n &= 16; \quad R^2 = 0.334; \quad S_{reg} = 0.715; \quad F_{statistic} = 0.251\end{aligned} \tag{2}$$

where n is the number of compounds, R^2 is the determination coefficient, S_{reg} is the standard deviation of regression, and $F_{statistic}$ is the Fisher statistic. The low determination coefficient value ($R^2 = 0.334$), the high values of standard error ($S_{reg} = 0.715$) and variance inflation factor (VIF > 10) lead to refuse the calculation of IC_{50}. The best way to deal with such a problem is to calculate variance inflation factor (VIF). We calculated VIF, which is a measure of multicollinearity, for each of the parameters involved in models. The VIF is defined as $1/(1 - R_i^2)$, where R_i is the multiple correlation coefficient of the ith independent variable on all of the other independent variables. A VIF 10 or more (no upper limit is defined) for large data sets indicates a collinearity problem. For small data sets, even VIFs of five or more (here also no upper limit is defined) can signify collinearity. On the other hand, the VIF value greater than 10 (Table 5) is associated with multicollinearity problem. Therefore, the variables with a high VIF are candidates for

Table 5 VIF[a] values for the QSAR equations

Independent variable	Equation 1a	Equation 2	Equation 3
Q_P	14.058	24.417	5.487
Q_N	3.767	7.451	3.709
$PL_{P=O}$	5.115	6.587	6.055
PL_{N-H}	2.021	4.829	3.898
E_{HOMO}	46.756	82.306	
E_{LUMO}	161.187	185.315	3.124
ω	231.713	307.941	
μ	3.416	4.923	3.762
log P	2.693	4.206	2.801
Mv	3.092	7.257	5.734

[a] $\mathrm{VIF} = 1/(1 - R_i^2)$; where R_i is the multiple correlation coefficient of the ith independent variable on all of the other independent variables

exclusion from the model [27]. Regression was significant; however, it gave high residuals for compounds **1**, **11** and **22**. As a result, a MLR was done excluding these three compounds from the data set using all the ten descriptors that gave Eq. 3.

$$\begin{aligned}\log(1/\mathrm{IC}_{50}) &= +0.128\log\ \mathrm{P} - 0.002\mu - 1.363Q_P + 23.768Q_N \\ &\quad + 2.841\mathrm{PL}_{P=O} - 31.446\mathrm{PL}_{N-H} - 61.586E_{HOMO} \\ &\quad - 33.712E_{LUMO} - 24.775\omega - 0.008\mathrm{Mv} + 71.121 \\ n &= 13;\quad R^2 = 0.992;\quad S_{reg} = 0.117;\quad F_{statistic} = 25.767\end{aligned} \tag{3}$$

The equation was significant with low residuals and low standard error of mean. The VIF value showed that ω and E_{HOMO} are highly inter correlated with E_{LUMO}. Therefore, a MLR was performed by removing ω and E_{HOMO}, which was correlated with E_{LUMO} and Eq. 4 was obtained as follows;

$$\begin{aligned}\log(1/\mathrm{IC}_{50}) &= +0.144\log\ P + 0.034\mu + 1.860Q_P + 36.554Q_N \\ &\quad + 3.284\mathrm{PL}_{P=O} - 29.078\mathrm{PL}_{N-H} \\ &\quad - 35.394E_{LUMO} - 0.006\mathrm{Mv} + 83.965 \\ n &= 13;\quad R^2 = 0.926;\quad S_{reg} = 0.256;\quad F_{statistic} = 6.257\end{aligned} \tag{4}$$

The correlating parameters have VIF < 10; thus, there is no collinearity problem (Table 5). In this equation, the inhibitory potency of AChE is influenced mainly by the electronic parameters with preferential order as $Q_N > E_{LUMO} > PL_{N-H} > PL_{P=O} > Q_P$ versus structural descriptors (log P, μ and Mv). From the QSAR model in Eq. 4, the molecular descriptors like an integrated net charge of nitrogen atom (Q_N), PL_{N-H} and E_{LUMO} proved important in defining the activity of the candidates. The correlation matrix was used to determine the interrelationship between the independent variables (Table 6). Table 6 shows that the majority of regression coefficients among showing that they were closely correlated. Therefore, orthogonalization of the molecular descriptors was conducted. Orthogonalization of molecular descriptors is undertaken to avoid collinearity among variables and model overfitting. The high interrelationships were observed between E_{LUMO} and Q_N ($r = -0.566$). A result was obtained from the above data; the high electrophilicity of the compounds, and thereby accepting electrons to its lowest unoccupied molecular orbital, would help them to improve the biological activity. Moreover, E_{LUMO} parameter controls the influence of the net charge of nitrogen atom of Tem derivatives in inhibition of AChE enzyme.

Conclusions

A series of temephos (Tem) derivatives (**1–22**) were synthesized and characterized. Also, the crystal structure of

Table 6 Correlation matrix for the anti-AChE parameters and the selected variables in Eq. (3)

Selected variables	Q_P	Q_N	$PL_{P=O}$	PL_{N-H}	E_{LUMO}	μ	log P	Mv
Q_P	1.000							
Q_N	−0.001	1.000						
$PL_{P=O}$	−0.838	−0.269	1.000					
PL_{N-H}	+0.385	+0.086	−0.213	1.000				
E_{LUMO}	−0.106	−0.566	+0.302	−0.321	1.000			
μ	0.276	+0.306	−0.442	+0.045	−0.595	1.000		
log P	0.131	−0.365	−0.065	−0.158	+0.568	−0.526	1.000	
Mv	−0.310	+0.665	+0.045	−0.439	−0.313	+0.040	−0.340	1.000

compounds **1** and **7** was investigated. The stabilizing energies (E^2) were calculated by NBO analysis of the crystal cluster **7**. The results of NBO analysis showed that the hydrogen bonding energy in P(1′)–O(1′)···(1)H–N(1) model (−72.15 kJ mol^{-1}) is higher than the value calculated for P(1)–O(1)···(1′)H–N(1′) (–45.67 kJ mol^{-1}). The compound **16** $(OC_2H_5)_2(O)P–NH(C_6H_4)SO_2(C_6H_4)NH–P(O)(OC_2H_5)_2$ versus human AChE displayed the most potent inhibitory activity. The insecticide activity of compounds **18**–**22** appraised for the elm leaf beetle (*Xanthogaleruca luteola Müll*) which the compound **18** $(C_6H_5)_2(O)P–NH(C_6H_4)O(C_6H_4)NH–P(O)(C_6H_5)_2$ had more effective than the other compounds in inhibition α-esterase of insect AChE enzyme. PCA–QSAR indicated that it was deduced that the frontier molecular orbital energy parameters (E_{HOMO}, E_{LUMO}, ω) in PC_1 are predominated from those related to electronic (Q_P, Q_N, $PL_{P=O}$ and $PL_{N–H}$) in PC_2 and structural parameters (log P and Mv) in PC_3 equation. MLR–QSAR models clarified that the molecular descriptors like an integrated net charge of nitrogen atom (Q_N), $PL_{N–H}$ and E_{LUMO} proved important in defining the activity of the candidates. E_{LUMO} parameter controls the influence of the net charge of nitrogen atom of Tem derivatives in inhibition of human AChE enzyme.

Acknowledgments The financial support of Tarbiat Modares, Guilan and Imam Hossein University's Research Council is gratefully acknowledged.

Supplementary data

CCDC 1027644 and 1027645 contain the supplementary crystallographic data for compounds **1** and **7**. These data can be obtained free of charge via http://www.ccdc.cam.ac.uk/conts/retrieving.html, or from the Cambridge Crystallographic Data Centre, 12 Union Road, Cambridge CB2 1EZ, UK; fax: (+44) 1223-336-033; or e-mail: deposit@ccdc.cam.ac.uk.

References

1. T.K. Olszewski, J. Gałęzowska, B. Boduszek, H. Kozłowski, Eur. J. Org. Chem. **21**, 3539 (2007)
2. V.M.R. Dos Santos, C.M.R. Sant Anna, G.E.M. Borja, A. Chaaban, W.S. Cortes, J.B.N. Da Costa, Bioorg. Chem. **35**, 68 (2007)
3. B. Kaboudin, S. Emadi, A. Hadizadeh, Bioorg. Chem. **37**, 101 (2009)
4. C. Fest, K.J. Schmidt, *The Chemistry of Organophosphorus Pesticides* (Springer, Berlin, 1982)
5. E.M. Lores, J.C. Moore, P. Moody, J. Clark, J. Forester, J. Knight, Bull. Environ. Contam. Toxicol. **35**, 308 (1985)
6. S.N. Tikar, A. Kumar, G.B.K.S. Prasad, S. Prakash, Parasitol. Res. **105**, 57 (2009)
7. B.K. Hackenberger, D.J. Perkusic, S. Stepic, Ecotoxicol. Environ. Saf. **71**, 583 (2008)
8. T.A. Ba-Omar, S. Al-Jardani, R. Victor, Tissue Cell **43**, 29 (2011)
9. T. Meiners, M. Hilker, Oecologia **112**, 87 (1997)
10. G.L. Ellman, C.K.D. Outney, V.R. Andres, M. Featherstone, Biochem. Pharmacol. **7**, 91 (1961)
11. PASS software, version 1.917, July (2005)
12. SPSS for Windows, Version 10.05. SPSS Inc., Bangalore (1999)
13. G.M. Sheldrick, Acta Crystallogr. **A64**, 112 (2008)
14. K. Gholivand, H.R. Mahzouni, Acta Crystallogr. **B67**, 238 (2011)
15. A.E. Reed, L.A. Curtiss, F. Weinhold, Chem. Rev. **88**, 899 (1988)
16. J.E. Carpenter, F. Weinhold, J. Mol. Struct. THEOCHEM. **169**, 41 (1988)
17. S.F. Boys, F. Bernardi, Mol. Phys. **19**, 553 (1970)
18. M.J. Frisch, G.W. Trucks, H.B. Schlegel, G.E. Scuseria, M.A. Robb, J.R. Cheeseman, J.A. Montgomery Jr., T. Vreven, K.N. Kudin, J.C. Burant, J.M. Millam, S.S. Iyengar, J. Tomasi, V. Barone, B. Mennucci, M. Cossi, G. Scalmani, N. Rega, G.A. Petersson, H. Nakatsuji, M. Hada, M. Ehara, K. Toyota, R. Fukuda, J. Hasegawa, M. Ishida, T. Nakajima, Y. Honda, O. Kitao, H. Nakai, M. Klene, X. Li, J.E. Knox, H.P. Hratchian, J.B. Cross, V. Bakken, C. Adamo, J. Jaramillo, R. Gomperts, R.E. Stratmann, O. Yazyev, A.J. Austin, R. Cammi, C. Pomelli, J.W. Ochterski, P.Y. Ayala, K. Morokuma, G.A. Voth, P. Salvador, J.J. Dannenberg, V.G. Zakrzewski, S. Dapprich, A.D. Daniels, M.C. Strain, O. Farkas, D.K. Malick, A.D. Rabuck, K. Raghavachari, J.B. Foresman, J.V. Ortiz, Q. Cui, A.G. Baboul, S. Clifford, J. Cioslowski, B.B. Stefanov, G. Liu, A. Liashenko, P. Piskorz, I. Komaromi, R.L. Martin, D.J. Fox, T. Keith, M.A. Al-Laham, C.Y. Peng, A. Nanayakkara, M. Challacombe, P.M.W. Gill, B. Johnson, W. Chen, M.W. Wong, C. Gonzalez, J.A. Pople, *Gaussian 03, Revision D.01* (Gaussian Inc, Wallingford, 2005)
19. C. Hansch, T. Fujita, J. Am. Chem. Soc. **86**, 1616 (1964)
20. E.B. de Melo, Eur. J. Med. Chem. **45**, 5817 (2010)
21. P.V. Hentenryck, *SAS '97*, Paris, France. Lecture Notes in Computer Science (1997)
22. J. Bernstein, R.E. Davis, L. Shimoni, N.L. Chang, Angew. Chem. Int. Ed. **34**, 1555 (1995)
23. K. Gholivand, A.A. Ebrahimi Valmoozi, H.R. Mahzouni, Acta Crystallogr. **B69**, 55 (2013)
24. A. Lagunin, A. Stepanchikova, D. Filimonov, V. Poroikov, Bioinform. Appl. Note **16**, 747 (2000)
25. R.A. Copeland, *Enzymes, a Practical Introduction to Structure, Mechanism, and Data Analysis*, 2nd edn. (John Wiley-VCH, New York, 2000)
26. S. Soltani, H. Abolhasani, A. Zarghi, A. Jouyban, Eur. J. Med. Chem. **45**, 2753 (2010)
27. J. Singh, B. Shaik, S. Singh, V.K. Agrawal, P.V. Khadikar, O. Deeb, C.T. Supuran, Chem. Biol. Drug Des. **71**, 244 (2008)